PAPER

Generation and stabilization of Bell states via repeated projective measurements on a driven ancilla qubit

To cite this article: L Magazzù *et al* 2018 *Phys. Scr.* **93** 064001

View the article online for updates and enhancements.

Related content

- What is the optimal way to prepare a Bell state using measurement and feedback?
Leigh Martin, Mahrud Sayrafi and K Birgitta Whaley

- Measures and applications of quantum correlations
Gerardo Adesso, Thomas R Bromley and Marco Cianciaruso

- Generating and protecting correlated quantum states under collective dephasing
Edoardo G Carnio, Andreas Buchleitner and Manuel Gessner

Generation and stabilization of Bell states via repeated projective measurements on a driven ancilla qubit

L Magazzù[1] , **J D Jaramillo**[1], **P Talkner**[1] **and P Hänggi**[1,2]

[1] Institute of Physics, University of Augsburg, D-86135 Augsburg, Germany
[2] Nanosystems Initiative Munich, Schellingstraße 4, D-80799 München, Germany

E-mail: luca.magazzu@physik.uni-augsburg.de

Abstract

A protocol is proposed to generate Bell states in two non-directly interacting qubits by means of repeated measurements of the state of a central ancilla connected to both qubits. An optimal measurement rate is found that minimizes the time to stably encode a Bell state in the target qubits, being of advantage in order to reduce detrimental effects from possible interactions with the environment. The quality of the entanglement is assessed in terms of the concurrence and the distance between the qubits state and the target Bell state is quantified by the fidelity.

(Some figures may appear in colour only in the online journal)

1. Introduction

Preparing entangled states is a basic requirement for many quantum technologies [1, 2], notably for quantum information [3] and quantum metrology [4, 5]. Being entanglement an exquisite non-classical feature, its quantification is of fundamental interest [6–8]. Several protocols to generate entangled states have been developed to date, including control of quantum dynamics [9–12] and engineered dissipation [13–22]. An intriguing route towards this goal is to exploit the quantum backaction of measurements performed on a part or on the whole system. In this context, different schemes have been proposed [23–28, 55] and implemented [29–31] which rely on the use of a parity meter on the collective state of two qubits. The introduction of a feedback control based on the readout of a continuous weak measurement of parity provides further means to entangle bipartite systems [32–35]. A parity meter of the state of two qubits, α and β, discriminates if they are in an even or odd parity collective state, associated to the two eigenvalues 1 and -1 of the parity operator $\sigma_z^\alpha \otimes \sigma_z^\beta$, respectively. Consider the one-qubit state $|+\rangle = (|\uparrow\rangle + |\downarrow\rangle)/\sqrt{2}$ expressed in the eigenbasis of σ_z. A parity measurement on the two-qubit system prepared in the separable joint state $|+_\alpha\rangle|+_\beta\rangle$ projects the system onto one of the Bell states $|\Phi^+\rangle = (|\uparrow\uparrow\rangle + |\downarrow\downarrow\rangle)/\sqrt{2}$ and $|\Psi^+\rangle = (|\downarrow\uparrow\rangle + |\uparrow\downarrow\rangle)/\sqrt{2}$, corresponding to even and odd parity outcome, respectively. An advantage of the class of schemes based on parity measurements is that they do not require direct interaction between the qubits, a feature that makes them suitable for linear optics setups, e.g., the scheme for quantum computing discussed in [36].

In practical implementations, the parity measurements may involve the coupling to an ancillary qubit upon which measurements are performed, and the use of multi-qubit gates to prepare the ancilla qubit as a parity meter [29, 30]. On the other hand, the action on the ancilla to drive the system state, allows for keeping the target qubits more isolated from the environment (which in general includes the measurement apparatus). In such a situation, the ancillary system can thus be considered as a so-called quantum actuator (see [37] and references therein) accomplishing the indirect control of the system state.

In the present work we exploit the idea of a shared ancilla driven by the measurement backaction [38–40] to circumvent the use of collective unitary gates to generate Bell states in a bipartite target system. Specifically, we encode and stabilize the Bell states in a couple of mutually non-interacting qubits (B and C) by repeated projective measurements of the state of
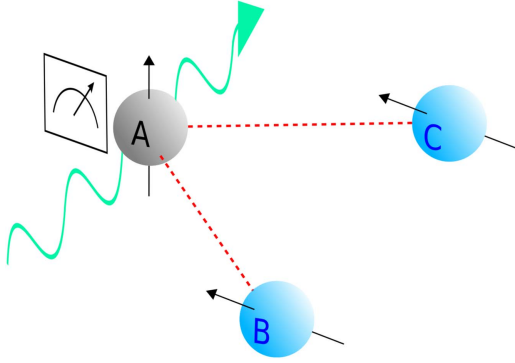
Figure 1. Two mutually non-interacting qubits (*B* and *C*) are coupled to a shared ancilla *A* whose state (σ_z) is projectively monitored. During the protocol, a control field acts on *A* triggered by a specific readout. We assume the qubits to be isolated from the environment.

a shared ancilla qubit (*A*) which may also driven by local control fields (see figure 1). The sequence of measurements is performed starting with the full system in the factorized state with the three qubits in the same spin state. A readily implementable form of feedback, i.e., a ramp of the control field on *A* triggered by a specific outcome of the measurement, ensures that in the ideal case of perfect isolation from the environment the protocol yields a Bell state with probability 1. Moreover, the sequence of outcomes of the measurements on *A*, unambiguously identifies the specific Bell state in which the target qubits *B* and *C* are left asymptotically. One can then switch among the four Bell states encoded in *BC* by addressing locally either *B* or *C* with a single qubit operation [41], an action that does not require proximity or interaction between the entangled qubits. The feasibility of our scheme benefits from the progress in rapid high-fidelity, single-shot readout in circuit QED, superconducting qubits, and spins in solid state systems [42–50].

By analyzing the results of the protocol with different inter-measurement times, we are able to identify the optimal rate of measurements to generate stable Bell states in a minimal amount of time. This is crucial for successfully producing a Bell state before the detrimental effects of environmental noise spoil the protocol [51]. We then use this optimal rate to examine how stable Bell states in the target qubits can be produced in a short time window, comprising ∼20 measurements on ancilla *A*, before the latter is disconnected leaving the target qubits isolated. We explicitly depict sample time evolutions of the density matrix, corresponding to different realizations of the measurement sequences.

2. Setup

The model considered in our protocol consists of an open one-dimensional chain comprised of three $1/2$-spins *A*, *B*, and *C* (the qubits, see figure 1). The central spin *A* plays the role of an ancilla and is connected to the measurement apparatus which projectively monitors its spin state in the *z*-direction. The ancilla *A* can be driven by a control field along the *z*-axis.

The target spins *B* and *C* interact exclusively with *A*. We assume that dephasing and relaxation effects from the environment do not affect the system, at least on the time scale of the protocol with optimal monitoring rate (see below). The inter-spin coupling and the control field are adjusted by control functions $u_J(t)$ and $u_h(t)$, respectively, both assuming values in [0,1].

The Hamiltonian reads:

$$H(t) = J_x u_J(t)\sigma_x^A(\sigma_x^B + \sigma_x^C) - h_z u_h(t)\sigma_z^A, \qquad (1)$$

where σ_j^i denote the Pauli spin operators ($j = x, y, z$) of spin *i*. Here the couplings J_x and h_z determine the magnitude of interaction and the field strength, respectively. The dynamics of the three qubit system between consecutive measurements is induced by the Hamiltonian in equation (1). Thus, the time evolution of the total density matrix ρ of the tripartite system *A*, *B*, *C* is governed by the Liouville–von Neumann equation

$$\dot{\rho}(t) = -\frac{\mathrm{i}}{\hbar}[H(t), \rho(t)]. \qquad (2)$$

Throughout the present work we scale energies and times with the coupling J_x which can be in practice very small, favoring the isolation of the target qubits, but at the expense of a longer duration of the protocol. Accordingly, we consider for the control field driving the ancilla the (maximal) value $h_z = 50\,J_x$.

The state of the three qubits (ancilla *A* and target qubits *B*, *C*) are expressed in the basis $|nml\rangle := |n_A\rangle|m_B\rangle|l_C\rangle$, where $n, m, l \in \{0, 1\}$ are the eigenvalues of the operators

$$\hat{Z}^i = (\mathbf{1}^i + \sigma_z^i)/2, \qquad (3)$$

with $i = A, B,$ and *C*, respectively. We consider repeated *projective* measurements of $\hat{Z}^A$ which are assumed to be instantaneous, meaning that they take place on a time scale which is much smaller than the dynamical time scales of the system. Each measurement on the ancilla projects the state of the full system into one of the eigensubspaces corresponding to the eigenvalues 0 and 1 of $\hat{Z}^A$.

In the next sections we study the time evolution of the system subject to repeated measurements of $\hat{Z}^A$, starting from the fully separable initial state $\rho_0 = |111\rangle\langle 111|$ with h_z set to zero. After each measurement, the density matrix evolves unitarily with respect to $H(t)$, until the next measurement is performed. The cycle is repeated for an overall time comprising several inter-measurement times.

3. Evolution under nonselective monitoring and optimal inter-measurement time.

In our protocol, measurements of the spin state of the ancilla *A* occur at equally-spaced times instants $t_n = n\tau$, where τ is the inter-measurement time and $n \geqslant 1$. The scope of the present section is to establish how the time needed to eventually reach an asymptotic state depends on τ. For this purpose, we study the evolution of the system undergoing a sequence of *nonselective* measurements in the absence of external fields, i.e., $u_h(t) = 0$, and with $u_J(t) = 1$. In a nonselective measurement the outcome
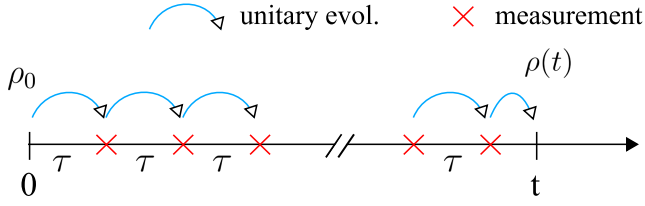
Figure 2. Scheme of the unitary evolution of the full system interrupted by the sequence of equally-spaced measurements of the state of qubit *A*. The time evolution between measurements is induced by the Hamiltonian (1) according to the Liouville–von Neumann equation (2).

is disregarded or simply not available, thus yielding only a probabilistic information about the post-measurement state of the system. This is in distinct contrast to the case of *selective* measurement where each measurement prepares the system in the eigenstate corresponding to the outcome of the measured operator. A nonselective measurement of $\hat{Z}^A$ reduces the state of the entire system to a probabilistic mixture of projections into the eigenstates $|0_A\rangle$ and $|1_A\rangle$ (see equation (3)). This transformation is provided by the action of the projectors $\Pi_i \equiv |i_A\rangle\langle i_A| \otimes \mathbf{1}_{BC}$ with $i \in \{0, 1\}$. Indeed, immediately after the *n*th nonselective measurement, taking place at time $t_n = n\tau$, the density matrix of the total system can be written as

$$\rho(t_n) = \Pi_0 U_n \rho(t_{n-1}) U_n^\dagger \Pi_0 + \Pi_1 U_n \rho(t_{n-1}) U_n^\dagger \Pi_1, \quad (4)$$

where U_n is the time evolution operator from t_{n-1} to t_n.

In the presence of repeated nonselective measurements, the density matrix at an arbitrary time *t* is calculated as follows. Starting at the initial time $t_0 = 0$ in the state $\rho_0 = |111\rangle\langle 111|$, the density matrix is propagated through equation (2) for a time span τ after which the coherences between *A* and the target qubits *B* and *C* are removed upon measuring the state of *A*, according to equation (4). Then, the post-measurement state $\rho(t_1)$ described by equation (4) is used as the initial condition for a further propagation up to time $t_2 = 2\tau$ where a second measurement takes place. The above sequence is repeated and the total number of measurements occurring up to time *t* is given by the integer part of t/τ. A scheme of this sequence is depicted in figure 2. We find that, for any non-pathological choice of the inter-measurement time τ, i.e., for inter-measurement times that do not match multiples of the free system periodicity, the asymptotic state

$$\rho^\infty = \frac{1}{2}|1_A\rangle\langle 1_A| \otimes |\Phi_{BC}^-\rangle\langle\Phi_{BC}^-| + \frac{1}{4}|1_A\rangle\langle 1_A| \otimes |\Phi_{BC}^+\rangle\langle\Phi_{BC}^+|$$
$$+ \frac{1}{4}|0_A\rangle\langle 0_A| \otimes |\Psi_{BC}^+\rangle\langle\Psi_{BC}^+| \quad (5)$$

is eventually reached, where the four Bell states are defined as

$$|\Phi_{BC}^\pm\rangle = \frac{1}{\sqrt{2}}(|11\rangle_{BC} \pm |00\rangle_{BC})$$
$$|\Psi_{BC}^\pm\rangle = \frac{1}{\sqrt{2}}(|10\rangle_{BC} \pm |01\rangle_{BC}). \quad (6)$$

Note that the Bell state $|\Psi_{BC}^-\rangle$ does not appear in equation (5). This is due to the particular initial condition chosen, as explained in appendix A. Inspection of equation (5) reveals that, once the
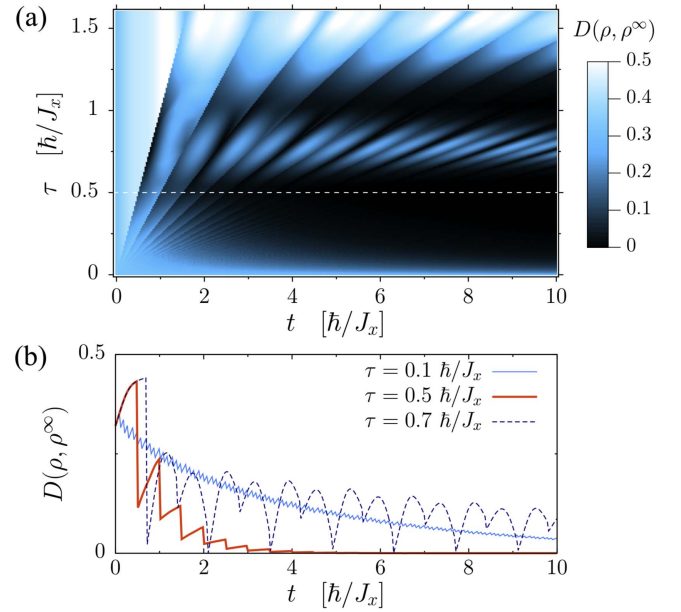

Figure 3. Time evolution of the full density matrix under repeated nonselective measurements. (a) Trace distance $D(\rho, \rho^\infty)$ between the time-evolved state $\rho \equiv \rho(t)$ and the asymptotic state ρ^∞ (see equation (5)) as a function of the actual time *t* and the inter-measurement time τ. For each value of τ the density matrix is propagated up to the final time $t = 10\,\hbar/J_x$ according to the sequence depicted in figure 2. The time evolution of the density matrix between measurements is obtained by numerically solving of the Liouville–von Neumann equation (2) with $u_h(t) = 0$ and $u_J(t) = 1$ in the Hamiltonian (1). At the measurement times the state of the system is transformed as prescribed by equation (4). The initial state is $\rho(0) = |111\rangle\langle 111|$. The horizontal line at $\tau = 0.5\,\hbar/J_x$ highlights the optimal inter-measurement time to rapidly relax to the asymptotic state. In the limit $\tau \to 0$ the system enters the quantum Zeno regime, as witnessed by the freezing of the trace distance from the asymptotic state at its initial value. (b) Trace distance *versus* time for three fixed values of τ. The red thick line corresponds to the optimal inter-measurement time.

asymptotic state is attained, a further measurement on *A*, with available outcome, yields for the target qubits *B* and *C* the Bell state $|\Psi_{BC}^+\rangle$ conditioned on the readout 0, which occurs with probability 1/4. On the other hand, the outcome 1 yields for the target qubits a probabilistic mixture of Bell states. In the following section and in appendix B, a protocol that also yields the other entangled states $|\Psi_{BC}^-\rangle$ and $|\Phi_{BC}^-\rangle$ as pure states is specified.

To establish the optimal inter-measurement time τ^* for which the asymptotic state ρ^∞ is reached in the least amount of time, we consider the trace distance between the time-evolved density operator $\rho(t)$ and the asymptotic state ρ^∞. This quantity is defined as

$$D(\rho(t), \rho^\infty) = \frac{1}{2} \mathrm{Tr}|\rho(t) - \rho^\infty|$$
$$= \frac{1}{2} \sum_i |\lambda_i|, \quad (7)$$

with λ_i denoting the eigenvalues of the Hermitian matrix $\rho(t) - \rho^\infty$.

The results for the trace distance as a function of time *t* and of the inter-measurement time τ are depicted in figure 3

for $u_h(t) = 0$ (no external field on A) and $u_J(t) = 1$ (constant qubits-ancilla coupling), see equation (1). The plot in figure 3(a) shows that an optimal inter-measurement time around the value $\tau^* = 0.5\,\hbar/J_x$ exists which corresponds to the minimal time t needed to relax to the final state ρ^∞ (see the horizontal dashed line). The curves depicted in figure 3(b) clearly show that, for $\tau = \tau^*$, the asymptotic state is reached after few measurements whereas deviations from this optimal inter-measurement time entail a considerably larger number of measurements. Indeed, in the limit of very small τ—well below the optimal level—the system enters the quantum Zeno regime, as witnessed by the freezing of the trace distance from the asymptotic state at its initial value (see the lower part of figure 3(a))[3]. On the other hand, upon increasing the inter-measurement time τ above the optimal value τ^* the measurements eventually synchronize with the periodicity of the free system so that oscillations persist for long evolution times around selected values of τ, as shown in the upper part of figure 3(a).

4. Selective evolution under projective measurements and feedback

Next we focus on the *selective* evolution of the system under the same sequence of repeated measurements on A detailed in section 3 (see figure 2). In this case the individual realizations of the time evolution of $\rho(t)$ determined by specific sequences of random outcomes of the measurements on A are considered. We show that the protocol converges to a factorized state with $|i_A\rangle\langle i_A| \otimes \rho^{BC}$, with the reduced system BC in a Bell state.

The evolution under selective measurements is calculated as follows: starting at $t = 0$ with the system in the state $\rho_0 = |111\rangle\langle 111|$, the full density matrix is evolved according to equation (2) for a time span τ. At time $t_1 = \tau$ the first measurement takes place yielding a random outcome $i \in \{0, 1\}$ generated with probability $\mathrm{Tr}[\rho(\tau)\Pi_i]$. The state of the system is then updated to the post-measurement state which is in turn used as the initial condition for a further unitary evolution of duration τ and so on. The process, with the measurements taking place at times $t_n = n\tau$, is depicted in figure 2. The explicit expression for the state immediately after the nth measurement with outcome $i_n \in \{0, 1\}$ is

$$\rho(t_n) = \frac{\Pi_{i_n} U_n \rho(t_{n-1}) U_n^\dagger \Pi_{i_n}}{\mathrm{Tr}[U_n \rho(t_{n-1}) U_n^\dagger \Pi_{i_n}]}. \quad (8)$$

The process described yields random realizations of the time evolution of the density matrix. The expression for the probability associated to a specific realization, i.e., to a specific readout sequence $(i_1,\ldots,i_n,\ldots)$, is given in appendix B (see equation (B.8)). In the absence of a control field ($h_z = 0$),

we find two possible behaviors: either the repeated measurements on A yield an uninterrupted sequence of 1's, and the system is asymptotically left in the state $|1_A\rangle|\Phi_{BC}^-\rangle$, or the sequence randomly flips between the two outcomes 1 and 0. In the latter case the state of the system flips between the two states $|1_A\rangle|\Phi^+\rangle$ and $|0_A\rangle|\Psi^+\rangle$. In appendix B we account for this behavior by explicitly considering actual realizations of the selective evolution.

To cope with the oscillating behavior taking place in a subset of the realizations of the protocol, a simple feedback scheme can be implemented which does not require particular precision in its execution. A ramp of the control field $-h_z u_h(t)\sigma_z^A$ acting on A (see equation (1)) is turned on triggered by the first readout of a 0 in the sequence of measurements. Specifically, the field is initially zero and is then switched on at the time t^* when a first detection of the state of A with outcome 0 occurs during the protocol. If no outcome 0 is found the field stays off during the evolution (see for example panel (a) of figure 4 below). Let t_F be the total duration of the protocol. The switching function is the smooth ramp

$$u_h(t) = \begin{cases} \Theta(t - t^*)\{1 - \cos[2\pi(t \\ -t^*)/t_F]\}/2, & t \leqslant (t^* + t_F)/2 \\ 1, & t > (t^* + t_F)/2 \end{cases} \quad (9)$$

see figures 4(a)–(c). The stabilizing effect on the oscillating sequences is due to the large value $(50\,J_x)$ of h_z which makes the field term dominating with respect to the interaction term in the Hamiltonian (1). As a result, a state with a definite eigenvalue of $\hat{Z}^A$, such as a post-measurement state, is approximately an eigenstate of the Hamiltonian and does not evolve on the time scales of the protocol. We note that this stabilizing effect—and thus the results in the present work—does not depend on the precise form of the ramp $u_h(t)$. The final part of the protocol consists in switching off the interaction strength $J_x u_J(t)$: the interaction is held constant $[u_J(t) = 1]$ throughout the protocol and is switched off at time t_F, i.e., $u_J(t \geqslant t_F) = 0$, after the target qubits B and C have reached a steady state.

In figure 4, the time evolution of the reduced density matrix $\rho^{BC}(t)$ under selective measurements is shown for three sample realizations of the protocol. These realizations end up with the target qubits left in different Bell states, corresponding to different sequences of the measurement readouts. The readout sequences are also shown for each sample time evolution along with the behavior of the control field acting on A. In the numerical simulations, the inter-measurement time τ is fixed at the optimal value $\tau^* = 0.5\,\hbar/J_x$ and the switch off takes place at $t_F = 10\,\hbar/J_x$, namely, after 20 measurements. A realization of the protocol leaves the target qubits in the Bell state $|\Phi_{BC}^-\rangle$ with probability $1/2$ or in one of the Bells states $|\Psi_{BC}^+\rangle$ and $|\Phi_{BC}^+\rangle$ with total probability $1/2$, (see the definitions in equation (6)). Although the protocol generates the Bell states non-deterministically, once the steady state is reached they are unambiguously identified by reading the sequence of outcomes of the measurements on A. Having identified the Bell state encoded in the system BC,

---

[3] In a different setup [52], measurements of the joint state of two qubits are proposed to entangle the qubits by exploiting the Zeno effect occurring at large measurement rates. Here, instead, we operate in the opposite regime where measurements at an appropriate, intermediate rate produce the fastest relaxation to a target state.
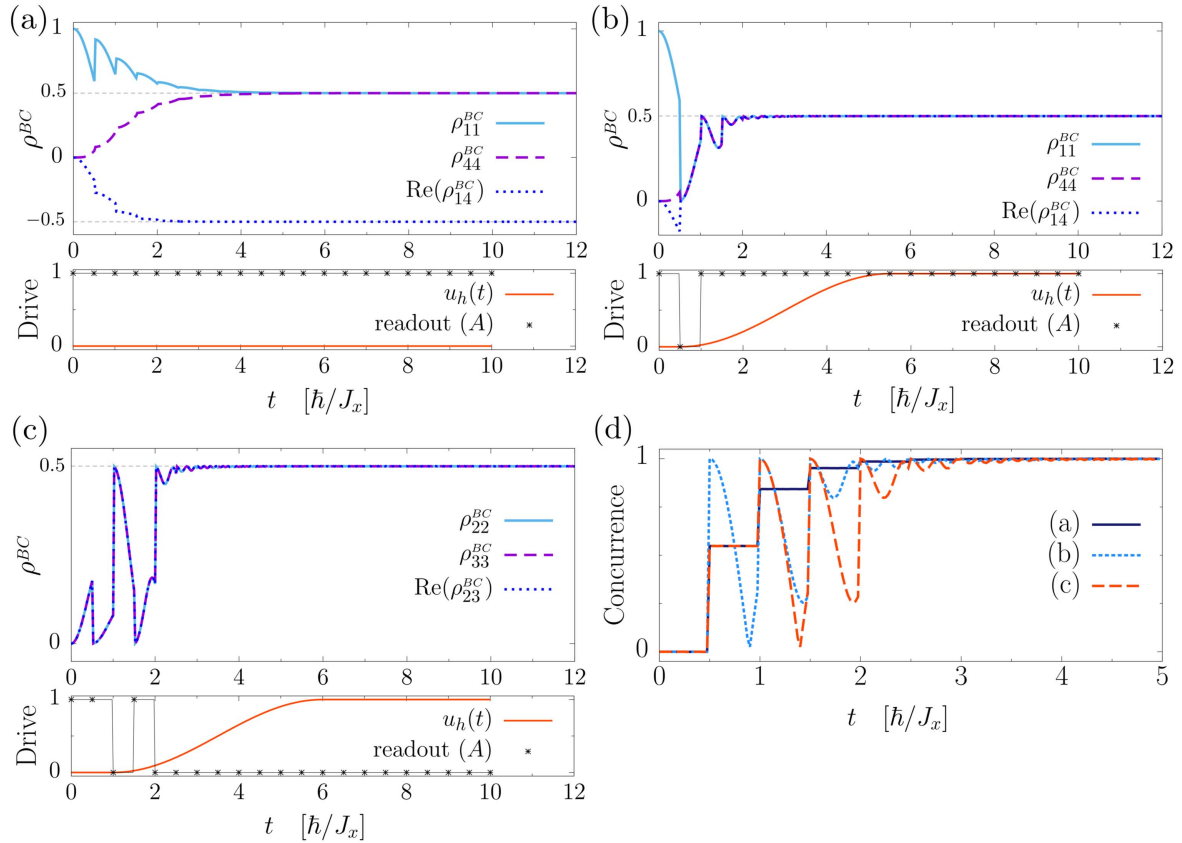
Figure 4. Time evolution of selected elements of the reduced density matrix $\rho^{BC}(t)$, for three sample realizations of the protocol with initial condition $|111\rangle$. Each trajectory leads to a different Bell state for the target system *BC*. Specifically, (a) $|\Phi_{BC}^{-}\rangle$, (b) $|\Phi_{BC}^{+}\rangle$ and (c) $|\Psi_{BC}^{+}\rangle$ (see figure 5 below). Persistent fluctuations in the trajectories (b) and (c) are suppressed by applying an external control field of the form $-h_z u_h(t)$, with $h_z = 50\,J_x$, to the ancilla *A*. Below each evolution we depict the corresponding sequence of outcomes from measuring the state of *A* and the time dependent function $u_h(t)$ of the control field (see equation (1)) acting on *A*. (d) Time evolution of the concurrence of $\rho^{BC}(t)$ for the trajectories (a)–(c). The inter-measurement time is set to the optimal value $\tau = 0.5\,\hbar/J_x$.

one can act *locally* on qubit *B* or *C*, by applying a rotation of the state of the qubit, to switch to a different Bells state [41].

A scheme of the protocol is provided in the upper panel of figure 5, where the three realizations in figures 4(a)–(c) are associated to the corresponding readout sequences and the final Bell state for the target qubits *B* and *C*. Note that, by using a different initial condition, the final Bell states associated to definite readout sequence can differ from the ones described here. This is exemplified in appendix C, where the protocol is carried out with the three qubits initially prepared in the state $|110\rangle$.

To study the degree of entanglement during the protocol, we evaluate the concurrence of the reduced density matrix of the target system *BC*. This quantity is defined as $\mathcal{C}[\rho^{BC}(t)] = \max(0, \lambda_1 - \lambda_2 - \lambda_3 - \lambda_4)$, where the λ_i's are the ordered eigenvalues of the matrix $\rho^{BC}(t)(\sigma_y^B \otimes \sigma_y^C)[\rho^{BC}(t)]^*(\sigma_y^B \otimes \sigma_y^C)$ [6, 7]. The concurrence takes values between zero and one, corresponding to non-entangled (zero) and maximally entangled states (one), respectively. The results are depicted in figure 4(d) for the three sample realizations displayed in panels (a)–(c). In addition, we confirm that the reduced two-qubit system *BC* is left in the specific Bell state corresponding to a particular readout sequence. This is done by calculating the fidelity

[53, 54], given by the expression

$$F[\rho^{BC}(t), \rho_\infty^{BC}] = \mathrm{Tr}[\sqrt{\sqrt{\rho^{BC}(t)}\,\rho_\infty^{BC}\,\sqrt{\rho^{BC}(t)}}], \quad (10)$$

where the referential density matrix ρ_∞^{BC} is chosen *a posteriori*, as the final state that corresponds to the readout sequence (see the upper panel of figure 5). The time evolutions of the fidelity for the sample evolutions in figure 4 are depicted in the lower panel of figure 5.

We conclude this section by noting that, in a realistic situation, environmental effects are present, especially on the ancilla qubit *A* which is connected to the meter. This makes the choice of the optimal time crucial in order to conclude the protocol before these detrimental effects spoil it. However, the realizations of the protocol in the classes depicted in figures 4(a) and (b) are expected to be more robust with respect to the environmental influence, as compared to those where the large control field acting on *A* freezes the system in the higher energy state $|0_A\rangle|\Psi_{BC}^+\rangle$. In this latter case, the large energy splitting may cause the decay $|0_A\rangle \rightarrow |1_A\rangle$ before the protocol is completed.

Alternatively, one may think of freezing the oscillations between $|1_A\rangle|\Phi^+\rangle$ and $|0_A\rangle|\Psi^+\rangle$ by the Zeno effect, namely by
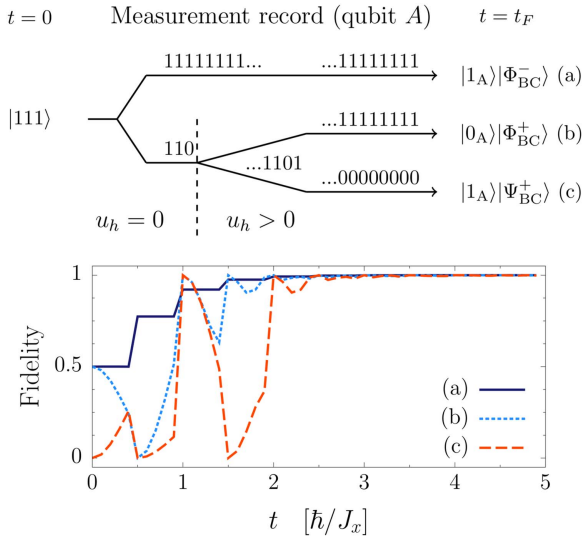
Figure 5. Upper panel—schematics of the protocol to generate Bell states in qubits B and C by a sequence of measurements on the ancilla qubit A, starting in the state $|111\rangle$. The scheme shows three different readout sequences with different resulting Bells states encoded in BC, corresponding to the three sample realizations in figures 4(b), (c). A smooth ramp of the control field $-h_z u_h(t)$, triggered by the first detection of a 0 in the outcomes' sequence (see figure 4), is applied to the ancilla in order to suppress the oscillatory behavior between $|1_A\rangle|\Phi_{BC}^+\rangle$ and $|0_A\rangle|\Psi_{BC}^+\rangle$ and converge to a definite result. Lower panel—fidelity of the trajectories depicted in figures 4(a)–(c) to the corresponding target Bell states.

suddenly let the inter-measurement time τ go to zero after a measurement on the ancilla with outcome 0.

5. Conclusions

With this work a simple protocol is presented for generating Bell states in a couple of qubits which do not interact directly. The qubits are entangled by means of repeated projective measurements of the state of a shared ancilla qubit. We have shown that the protocol yields a definite and stable Bell state, starting from the completely factorized state $|111\rangle$ of the full system. This is attained by acting on the ancilla with a suitable form of feedback, namely a ramp of a control field (see equation (9)), triggered by a specific readout of the ancilla state. The backaction of the repeated measurements asymptotically yields a stationary state of the form $|i_A\rangle|\varphi_{BC}\rangle$, with $i \in \{0, 1\}$ and $|\varphi_{BC}\rangle \in \{|\Phi_{BC}^-\rangle, |\Psi_{BC}^+\rangle, |\Phi_{BC}^+\rangle\}$, where the Bell state is unambiguously identified by reading the sequence of measurement outcomes of the ancilla.

Acknowledgments

Table A1. Repeated nonselective measurements in the absence of external fields—asymptotic mixed density matrix for eight initial configurations.

Init. state	ρ^∞
$\|111\rangle$ $\|100\rangle$	Equation (5)
$\|110\rangle$ $\|101\rangle$	Equation (A.3)
$\|011\rangle$ $\|000\rangle$	Equation (5) with $\|1_A\rangle \leftrightarrow \|0_A\rangle$
$\|010\rangle$ $\|001\rangle$	Equation (A.3) with $\|1_A\rangle \leftrightarrow \|0_A\rangle$

Appendix A. Asymptotic state for nonselective repeated measurements with different initial conditions

To gain insight in the reasons why, with the chosen initial separable state

$$|111\rangle = \frac{1}{\sqrt{2}}|1_A\rangle(|\Phi_{BC}^+\rangle + |\Phi_{BC}^-\rangle), \qquad (A.1)$$

the sequence of nonselective measurement considered in section 3 ends up with asymptotic state in equation (5), it is sufficient to note that the Hamiltonian (1), in the absence of control fields and with constant interaction strength, can be written as

$$H(t) = 2J_x \sigma_x^A(|\Phi_{BC}^+\rangle\langle\Psi_{BC}^+| + |\Psi_{BC}^+\rangle\langle\Phi_{BC}^+|). \qquad (A.2)$$

The state $|1_A\rangle|\Phi_{BC}^-\rangle$ is an eigenstate of the Hamiltonian and the only states involved that are connected by a nonzero transition amplitude are $|1_A\rangle|\Phi_{BC}^+\rangle$ and $|0_A\rangle|\Psi_{BC}^+\rangle$. Thus, with the chosen initial state, the probability to get the target qubits in the Bell state $|\Psi_{BC}^-\rangle$ is zero, as the dynamics induced by Hamiltonian (A.2) is confined to the subspace spanned by $\{|1_A\rangle|\Phi_{BC}^-\rangle, |1_A\rangle|\Phi_{BC}^+\rangle, |0_A\rangle|\Psi_{BC}^+\rangle\}$ and the measurements on A do not affect this feature. On the other hand, by starting with a different initial state, as for example $|110\rangle = |1_A\rangle(|\Psi_{BC}^+\rangle + |\Psi_{BC}^-\rangle)/\sqrt{2}$, the asymptotic state reads

$$\rho^\infty = \frac{1}{2}|1_A\rangle\langle1_A| \otimes |\Psi_{BC}^-\rangle\langle\Psi_{BC}^-|$$
$$+ \frac{1}{4}|1_A\rangle\langle1_A| \otimes |\Psi_{BC}^+\rangle\langle\Psi_{BC}^+|$$
$$+ \frac{1}{4}|0_A\rangle\langle0_A| \otimes |\Phi_{BC}^+\rangle\langle\Phi_{BC}^+|, \qquad (A.3)$$

(see equation (5)). A complete list of the asymptotic states attained by starting in each of the (computational) basis states is shown in table A1.
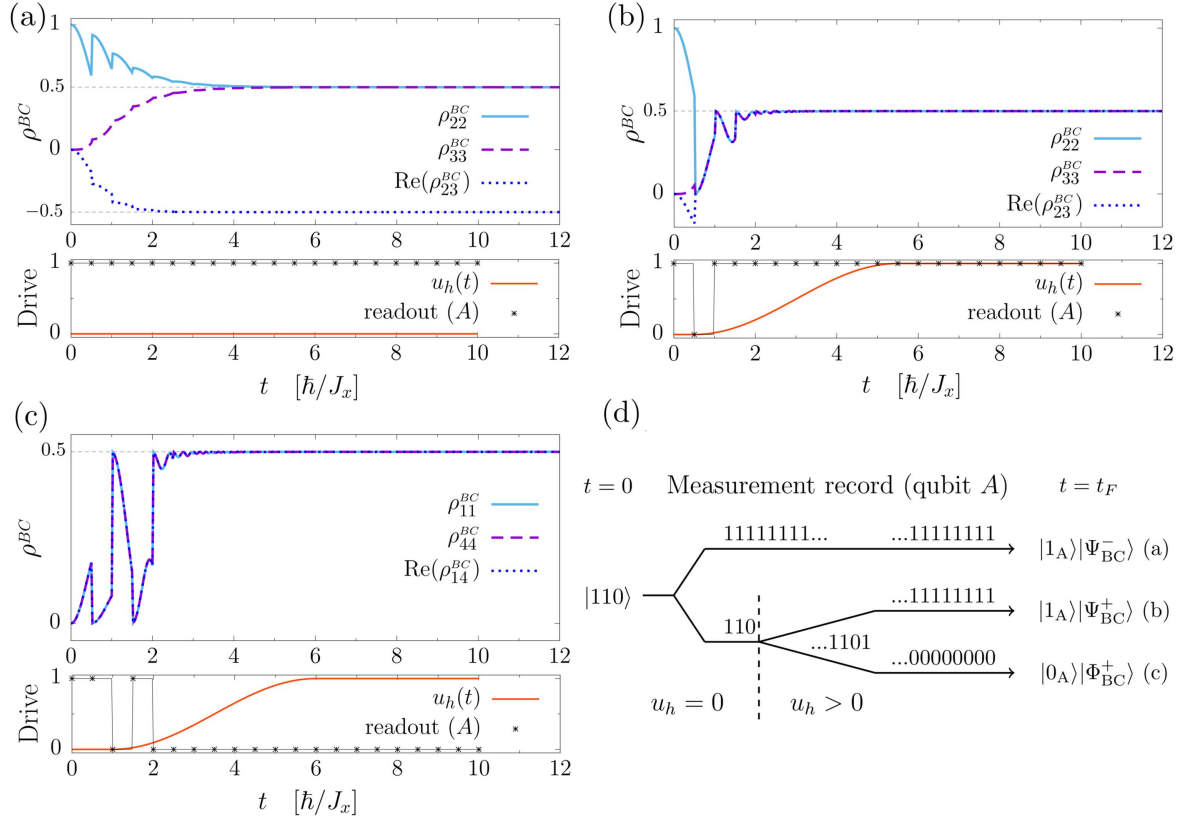
Figure C1. Time evolution of selected elements of the reduced density matrix $\rho^{BC}(t)$ and scheme of the protocol. Each of the three sample realizations of the protocol starts with the system in the state $|110\rangle$ and leads to a different Bell state for the target system B, C. Specifically, (a) $|\Psi_{BC}^-\rangle$, (b) $|\Psi_{BC}^+\rangle$ and (c) $|\Phi_{BC}^+\rangle$. Persistent fluctuations in the trajectories (b) and (c) are suppressed by applying an external control field of the form $-h_z u_h(t)$, with $h_z = 50\,J_x$, to the ancilla A. Below each evolution we depict the corresponding sequence of outcomes from measuring the state of A and the time dependent control function $u_h(t)$. The inter-measurement time is set to the optimal value $\tau = 0.5\,\hbar/J_x$. (d) Scheme of the readout sequences and final Bell states corresponding to panels (a)–(c) (see figure 5).

To gain an intuition on how the entries in the table are obtained, let us introduce the map $\mathcal{M}$ that propagates the density matrix for a time span τ and then applies a non-selective measurement on the ancilla. This map is defined by the action

$$\rho(t_n) = \Pi_0 U_n \rho(t_{n-1}) U_n^\dagger \Pi_0 + \Pi_1 U_n \rho(t_{n-1}) U_n^\dagger \Pi_1$$
$$\equiv \mathcal{M}[\rho(t_{n-1})]. \tag{A.4}$$

Then, the asymptotic state is given by

$$\rho^\infty = \lim_{n \to \infty} \mathcal{M}^n[\rho_0]. \tag{A.5}$$

Now, let $\mathcal{F}_j$ be the operation that flips the state of spin $j \in \{A, B, C\}$ in the computational basis (the eigenbasis of $\hat{Z}^j$). For $j \in \{B, C\}$, both the Hamiltonian and the projectors Π_i are invariant under such operation, we have

$$\mathcal{M}^n[\mathcal{F}_B \rho_0] = \mathcal{F}_B \mathcal{M}^n[\rho_0], \tag{A.6}$$

and similarly $\mathcal{M}^n[\mathcal{F}_C \rho_0] = \mathcal{F}_C \mathcal{M}^n[\rho_0]$ and $\mathcal{M}^n[\mathcal{F}_B \mathcal{F}_C \rho_0] = \mathcal{F}_B \mathcal{F}_C \mathcal{M}^n[\rho_0]$. It follows that flipping the spin of either B or C in the initial state $\rho_0 = |111\rangle\langle111|$ returns the asymptotic state in equation (5) with the spin of B or C flipped, i.e., equation (A.3). On the other hand, flipping both the spins of B and C in the initial state returns the asymptotic state (5) itself,

because $\mathcal{F}_B \mathcal{F}_C \rho^\infty = \rho^\infty$. The above reasoning accounts for the first two rows of table A1.

In a similar way, by writing $\sigma^A = |0_A\rangle\langle1_A| + |1_A\rangle\langle0_A|$ we see that the Hamiltonian is invariant under the action of $\mathcal{F}_A$ and that $\mathcal{F}_A \Pi_{0(1)} = \Pi_{1(0)}$, which entails $\mathcal{M}^n[\mathcal{F}_A \rho_0] = \mathcal{F}_A \mathcal{M}^n[\rho_0]$ (see equation (A.4)). This accounts for the last two rows of table A1.

Appendix B. Details of the selective evolution

Let us inspect the actual realizations of the time evolution given by repeatedly measuring the state of A in a selective fashion, starting from the state $|111\rangle$ in the absence of control fields, $u_h(t) = 0$. The action of the time evolution operator induced by the Hamiltonian (A.2) for a time span τ is

$$U(\tau)|111\rangle = \frac{1}{\sqrt{2}}|1_A\rangle(|\Phi_{BC}^-\rangle + a|\Phi_{BC}^+\rangle) + \frac{b}{\sqrt{2}}|0_A\rangle|\Psi_{BC}^+\rangle, \tag{B.1}$$

with $|a|^2 + |b|^2 = 1$, where a and b depend on τ. The first measurement on the ancilla collapses this evolved state into

one of the two alternative outcomes

$$|\phi_{(1)}\rangle = |1_A\rangle(|\Phi_{BC}^-\rangle + a|\Phi_{BC}^+\rangle)/\mathcal{N}_1 \qquad \text{prob} = \mathcal{N}_1^2/2$$
$$|\phi_{(0)}\rangle = |0_A\rangle|\Psi_{BC}^+\rangle \qquad\qquad\qquad \text{prob} = |b|^2/2,$$
(B.2)

where the indexes $(1/0\ldots)$ are used for bookkeeping the sequence of outcomes and $\mathcal{N}_n = \sqrt{1 + |a|^{2n}}$. Then, evolving the above states for another time span τ we get

$$U(\tau)|\phi_{(1)}\rangle = |1_A\rangle(|\Phi_{BC}^-\rangle + a^2|\Phi_{BC}^+\rangle)/\mathcal{N}_1 + ab|0_A\rangle|\Psi_{BC}^+\rangle/\mathcal{N}_1,$$
(B.3)

$$U(\tau)|\phi_{(0)}\rangle = a|0_A\rangle|\Psi_{BC}^+\rangle + b|1_A\rangle|\Phi_{BC}^+\rangle.$$
(B.4)

Upon measuring again the state of A the following two couples of alternative outcomes arise

$$\begin{cases} |\phi_{(11)}\rangle = |1_A\rangle(|\Phi_{BC}^-\rangle + a^2|\Phi_{BC}^+\rangle)/\mathcal{N}_2 & \text{prob} = \mathcal{N}_2^2/\mathcal{N}_1^2 \\ |\phi_{(10)}\rangle = |0_A\rangle|\Psi_{BC}^+\rangle & \text{prob} = |ab|^2/\mathcal{N}_1^2 \end{cases}$$
(B.5)

$$\begin{cases} |\phi_{(01)}\rangle = |1_A\rangle|\Phi_{BC}^+\rangle & \text{prob} = |b|^2 \\ |\phi_{(00)}\rangle = |0_A\rangle|\Psi_{BC}^+\rangle & \text{prob} = |a|^2 \end{cases}$$
(B.6)

and so on. From this behavior it is clear that, for $a \neq 1$, i.e., if τ is not a multiple of the period of the unitary evolution, a long sequence of outcomes 1 will yield the stabilized state $|1_A\rangle|\Phi_{BC}^-\rangle$, meaning that a further measurement will leave the system in this same state with probability ~ 1. On the other hand, the presence of zeroes in the readout sequences entails oscillations between $|1_A\rangle|\Phi_{BC}^+\rangle$ and $|0_A\rangle|\Psi_{BC}^+\rangle$ which last indefinitely. This behavior is very close to what is found in [55] by simulating the repeated parity measurements in a couple of double quantum dot qubits. The probability associated to a specific sequence of outcomes $(i_1, i_2, \ldots, i_N)$, where $i_n \in \{0, 1\}$, is given by

$$P(i_1, i_2, \ldots, i_N)$$
$$= \text{Tr}[\Pi_{i_N} U_N \ldots \Pi_{i_2} U_2 \Pi_{i_1} U_1 \rho_0 U_1^\dagger \Pi_{i_1} U_2^\dagger \Pi_{i_2} \ldots U_N^\dagger \Pi_{i_N}],$$
(B.7)

where, as in equation (4), U_n is the time evolution operator from t_{n-1} to t_n. By extrapolating from the sequence in equations (B.1)–(B.6) one sees that the probability to obtain an interrupted sequence of n readouts 1 is

$$P(1, \ldots, 1) = \frac{\mathcal{N}_1}{2}\frac{\mathcal{N}_2}{\mathcal{N}_1} \ldots \frac{\mathcal{N}_n}{\mathcal{N}_{n-1}} = \frac{1}{2}\frac{\mathcal{N}_n}{\mathcal{N}_{n-1}} \quad \xrightarrow{n \gg 1} \quad \frac{1}{2}.$$
(B.8)

Appendix C. Realizations of the protocol with a different initial condition

In figure C1 we depict three sample realizations of the protocol detailed in section 4 starting in the factorized state $|110\rangle = |1_A\rangle(|\Psi_{BC}^+\rangle + |\Psi_{BC}^-\rangle)/\sqrt{2}$. A schematics of the protocol's outcomes and readout sequences is also shown.

ORCID iDs

L Magazzù ● https://orcid.org/0000-0002-4377-8387

References

[1] Schleich W P 2001 *Quantum Optics in Phase Space* (Berlin: Wiley-VCH)
[2] O'Brien J L, Furusawa A and Vučković J 2009 Photonic quantum technologies *Nat. Photon.* **3** 687
[3] Horodecki R, Horodecki P, Horodecki M and Horodecki K 2009 Quantum entanglement *Rev. Mod. Phys.* **81** 865–942
[4] Giovannetti V, Lloyd S and Maccone L 2011 Advances in quantum metrology *Nat. Photon.* **5** 222
[5] Tóth G and Apellaniz I 2014 Quantum metrology from a quantum information science perspective *J. Phys. A: Math. Theor.* **47** 424006
[6] Hill S and Wootters W K 1997 Entanglement of a pair of quantum bits *Phys. Rev. Lett.* **78** 5022–5
[7] Wootters W K 1998 Entanglement of formation of an arbitrary state of two qubits *Phys. Rev. Lett.* **80** 2245–8
[8] Dahl J P, Mack H, Wolf A and Schleich W P 2006 Entanglement versus negative domains of Wigner functions *Phys. Rev.* A **74** 042323
[9] Steffen M, Ansmann M, Bialczak R C, Katz N, Lucero E, McDermott R, Neeley M, Weig E M, Cleland A N and Martinis J M 2006 Measurement of the entanglement of two superconducting qubits via state tomography *Science* **313** 1423–5
[10] Galve F, Zueco D, Kohler S, Lutz E and Hänggi P 2009 Entanglement resonance in driven spin chains *Phys. Rev.* A **79** 032332
[11] Galve F, Zueco D, Reuther G M, Kohler S and Hänggi P 2009 Creation and manipulation of entanglement in spin chains far from equilibrium *Eur. Phys. J. Spec. Top.* **180** 237–46
[12] Blattmann R, Krenner H J, Kohler S and Hänggi P 2014 Entanglement creation in a quantum-dot-nanocavity system by fourier-synthesized acoustic pulses *Phys. Rev.* A **89** 012327
[13] Plenio M B and Huelga S F 2002 Entangled light from white noise *Phys. Rev. Lett.* **88** 197901
[14] Verstraete F, Wolf M M and Cirac J I 2009 Quantum computation and quantum-state engineering driven by dissipation *Nat. Phys.* **5** 633
[15] Zueco D, Reuther G M, Hänggi P and Kohler S 2010 Entanglement and disentanglement in circuit QED architectures *Physica* E **42** 363–8
[16] Li P-B, Gao S-Y, Li H-R, Ma S-L and Li F-L 2012 Dissipative preparation of entangled states between two spatially separated nitrogen-vacancy centers *Phys. Rev.* A **85** 042306
[17] Leghtas Z, Vool U, Shankar S, Hatridge M, Girvin S M, Devoret M H and Mirrahimi M 2013 Stabilizing a Bell state of two superconducting qubits by dissipation engineering *Phys. Rev.* A **88** 023849
[18] Kimchi-Schwartz M E, Martin L, Flurin E, Aron C, Kulkarni M, Tureci H E and Siddiqi I 2016 Stabilizing entanglement via symmetry-selective bath engineering in superconducting qubits *Phys. Rev. Lett.* **116** 240503
[19] Benito M, Schuetz M J A, Cirac J I, Platero G and Giedke G 2016 Dissipative long-range entanglement generation between electronic spins *Phys. Rev.* B **94** 115404
[20] Reiter F, Reeb D and Sørensen A S 2016 Scalable dissipative preparation of many-body entanglement *Phys. Rev. Lett.* **117** 040501

[21] Li X-X, Li P-B, Ma S-L and Li F-L 2017 Preparing entangled states between two NV centers via the damping of nanomechanical resonators *Sci. Rep.* **7** 14116

[22] Li D X, Shao X Q and Yi X X 2017 Entangled-state preparation by dissipation, dispersive coupling, and quantum Zeno dynamics *Opt. Lett.* **42** 3904–7

[23] Beenakker C W J, DiVincenzo D P, Emary C and Kindermann M 2004 Charge detection enables free-electron quantum computation *Phys. Rev. Lett.* **93** 020501

[24] Engel H-A and Loss D 2005 Fermionic Bell-state analyzer for spin qubits *Science* **309** 586

[25] Ruskov R and Korotkov A N 2003 Entanglement of solid-state qubits by measurement *Phys. Rev.* B **67** 241305

[26] Kolli A, Lovett B W, Benjamin S C and Stace T M 2006 All-optical measurement-based quantum-information processing in quantum dots *Phys. Rev. Lett.* **97** 250504

[27] Hill C and Ralph J 2008 Weak measurement and control of entanglement generation *Phys. Rev.* A **77** 014305

[28] Williams N S and Jordan A N 2008 Entanglement genesis under continuous parity measurement *Phys. Rev.* A **78** 062322

[29] Pfaff W, Taminiau T H, Robledo L, Bernien H, Markham M, Twitchen D J and Hanson R 2012 Demonstration of entanglement-by-measurement of solid-state qubits *Nat. Phys.* **9** 29

[30] Saira O-P, Groen J P, Cramer J, Meretska M, de Lange G and DiCarlo L 2014 Entanglement genesis by ancilla-based parity measurement in 2D circuit QED *Phys. Rev. Lett.* **112** 070502

[31] Roch N, Schwartz M E, Motzoi F, Macklin C, Vijay R, Eddins A W, Korotkov A N, Whaley K B, Sarovar M and Siddiqi I 2014 Observation of measurement-induced entanglement and quantum trajectories of remote superconducting qubits *Phys. Rev. Lett.* **112** 170501

[32] Chantasri A, Kimchi-Schwartz M E, Roch N, Siddiqi I and Jordan A N 2016 Quantum trajectories and their statistics for remotely entangled quantum bits *Phys. Rev.* X **6** 041052

[33] Martin L, Sayrafi M and Whaley K B 2017 What is the optimal way to prepare a Bell state using measurement and feedback? *Quantum Sci. Technol.* **2** 044006

[34] Ristè D, Dukalski M, Watson C A, de Lange G, Tiggelman M J, Blanter Ya M, Lehnert K W, Schouten R N and DiCarlo L 2013 Deterministic entanglement of superconducting qubits by parity measurement and feedback *Nature* **502** 350

[35] Meyer zu Rheda C, Haack G and Romito A 2014 On-demand maximally entangled states with a parity meter and continuous feedback *Phys. Rev.* B **90** 155438

[36] Knill E, Laflamme R and Milburn G J 2001 A scheme for efficient quantum computation with linear optics *Nature* **409** 46

[37] Layden D, Martín-Martínez E and Kempf A 2016 Universal scheme for indirect quantum control *Phys. Rev.* A **93** 040301

[38] Nakazato H, Unoki M and Yuasa K 2004 Preparation and entanglement purification of qubits through Zeno-like measurements *Phys. Rev.* A **70** 012303

[39] Wu L-A, Lidar D A and Schneider S 2004 Long-range entanglement generation via frequent measurements *Phys. Rev.* A **70** 032322

[40] Compagno G, Messina A, Nakazato H, Napoli A, Unoki M and Yuasa K 2004 Distillation of entanglement between distant systems by repeated measurements on an entanglement mediator *Phys. Rev.* A **70** 052316

[41] Preskill J 2018 Lecture Notes on Quantum Computation http://theory.caltech.edu/people/preskill/ph229/

[42] Mallet F, Ong F R, Palacios-Laloy A, Nguyen F, Bertet P, Vion D and Esteve D 2009 Single-shot qubit readout in circuit quantum electrodynamics *Nat. Phys.* **5** 791

[43] Morello A *et al* 2010 Single-shot readout of an electron spin in silicon *Nature* **467** 687

[44] Neumann P, Beck J, Steiner M, Rempp F, Fedder H, Hemmer P R, Wrachtrup J and Jelezko F 2010 Single-shot readout of a single nuclear spin *Science* **329** 542

[45] Robledo L, Childress L, Bernien H, Hensen B, Alkemade P F A and Hanson R 2011 High-fidelity projective read-out of a solid-state spin quantum register *Nature* **477** 574

[46] Pla J J, Tan K Y, Dehollain J P, Lim W H, Morton J J L, Zwanenburg F A, Jamieson D N, Dzurak A S and Morello A 2013 High-fidelity readout and control of a nuclear spin qubit in silicon *Nature* **496** 334

[47] Delteil A, Gao W, Fallahi P, Miguel-Sanchez J and Imamoğlu A 2014 Observation of quantum jumps of a single quantum dot spin using submicrosecond single-shot optical readout *Phys. Rev. Lett.* **112** 116802

[48] Krantz P, Bengtsson A, Simoen M, Gustavsson S, Shumeiko V, Oliver W D, Wilson C M, Delsing P and Bylander J 2016 Single-shot read-out of a superconducting qubit using a Josephson parametric oscillator *Nat. Commun.* **7** 11417

[49] Walter T *et al* 2017 Rapid high-fidelity single-shot dispersive readout of superconducting qubits *Phys. Rev. Appl.* **7** 054020

[50] Zajac D M, Sigillito A J, Russ M, Borjans F, Taylor J M, Burkard G and Petta J R 2018 Resonantly driven CNOT gate for electron spins *Science* **359** 439–42

[51] Wong-Campos J D, Moses S A, Johnson K G and Monroe C 2017 Demonstration of two-atom entanglement with ultrafast optical pulses *Phys. Rev. Lett.* **119** 230501

[52] Wang X-B, You J Q and Nori F 2008 Quantum entanglement via two-qubit quantum Zeno dynamics *Phys. Rev.* A **77** 062339

[53] Uhlmann A 1976 The 'transition probability' in the space of a *-algebra *Rep. Math. Phys.* **9** 273–9

[54] Jozsa R 1994 Fidelity for mixed quantum states *J. Mod. Opt.* **41** 2315–23

[55] Trauzettel B, Jordan A N, Beenakker C W J and Büttiker M 2006 Parity meter for charge qubits: an efficient quantum entangler *Phys. Rev.* B **73** 235331